Journal of Electroceramics, 13, 645–651, 2004

Kinetics of Oxygen Incorporation into $SrTiO_3$ Investigated by Frequency-Domain Analysis

S.F. WAGNER,* W. MENESKLOU, TH. SCHNEIDER & E. IVERS-TIFFÉE
Institut für Werkstoffe der Elektrotechnik, Universität Karlsruhe (TH), Adenauerring 20 b, 76131 Karlsruhe, Germany

Submitted February 14, 2003; Revised February 15, 2004; Accepted February 18, 2004

Abstract. The kinetics of oxygen incorporation are of fundamental importance for an application of acceptor doped strontium titanate as a resistive-type oxygen sensor. The electrical conductance of the sample depends on the ambient oxygen partial pressure pO_2 due to oxygen exchange between gas phase and solid state which leads to a flow of charge carriers. The kinetics of the incorporation process can be separated into two steps: the oxygen surface transfer and the subsequent bulk diffusion of oxygen vacancies. The rate of the slower step determines the kinetics of the overall incorporation process and thus the sensor's response behavior.

A method for the investigation of the kinetic behavior is presented which is based on a frequency-domain analysis. In the underlying model, a $SrTiO_3$ single crystal is exposed to a harmonically modulated pO_2. This leads to a modulation of the sample's electrical conductance. By way of calculation, it is shown that the shape of the frequency response clearly allows to distinguish whether the kinetics of oxygen incorporation are determined either by bulk diffusion or by surface transfer.

The experimental validation of this model is demonstrated by investigations performed on slightly acceptor doped $SrTiO_3$ single crystals of various thicknesses in a kinetic measurement setup at different temperatures.

Keywords: strontium titanate, resistive-type oxygen sensor, kinetics, surface transfer, bulk diffusion

1. Introduction

Strontium titanate is a suitable material for a resistive-type high temperature ($T > 700^{\circ}C$) oxygen sensor which may be applied e.g. in automotive exhaust gas monitoring. Its electrical conductivity σ depends on the ambient oxygen partial pressure pO_2. The defect chemistry of $SrTiO_3$ has been treated at length, theoretically as well as experimentally, e.g. by [1–11]. Owing to different electrochemical potentials of the oxygen species involved, an oxygen exchange between gas phase and solid state occurs. The following treatment shall confine itself to the case of oxidizing conditions where the solid is exposed to an oxygen-rich atmosphere: Oxygen from the gas phase is incorporated into the solid, occupying oxygen vacancies $V_O^{\cdot\cdot}$ (twice ionized at the temperatures under consideration), thus forming regular oxygen ions in the anion sublattice. In Kröger-Vink notation this reaction reads:

$$\tfrac{1}{2}\,O_2 + V_O^{\cdot\cdot} \rightarrow O_O^x + 2h^{\cdot} \tag{1}$$

The resulting flow of charge carriers associated with the bulk diffusion of $V_O^{\cdot\cdot}$ in order to maintain electroneutrality [4] gives rise to a change of the material's electrical conductivity σ. Electronic contributions prevail, under oxidizing conditions the current is carried mainly by holes (defect electrons) $h^{\cdot}$, resulting in p-type conductivity. Once electrochemical equilibrium between gas phase and solid is established, the relationship $\sigma(pO_2, T)$ is well-defined:

$$\sigma \propto e^{-\left(E_A/kT\right)} pO_2^m \tag{2}$$

The first r.h.s. factor describes the temperature (T) dependence, E_A denoting an activation energy. Oxygen partial pressure dependence is described by the second factor. The value of the sensitivity m depends on the dominant type of bulk defect.

*To whom all correspondence should be addressed. E-mail: stefan.wagner@iwe.uni-karlsruhe.de

In this paper however, we shall turn our attention to the non-equilibrium situation. The response behavior of the sample is determined by the kinetics of equilibration, experimentally benchmarked by the response times t_{90} during which the sample obtains 90% of its final conductance value in response to a sudden pO_2 jump. The commonly used time-domain method for the measurement of t_{90} times, however, suffers from experimental limitations. In contrast, an alternative technique developed by Tragut et al. [12, 13] which is based on a frequency-domain analysis not only allows the determination of very short response times (in the order of milliseconds) but, interestingly, also an in situ investigation of the kinetic behavior the sample shows in response to a pO_2 change. The underlying model shall be presented in the following.

2. Frequency-Domain Analysis: Model

The oxygen incorporation process of Eq. (1) can be subdivided into various consecutive transport and electrochemical reaction steps, such as: (i) O_2 transport through a gas boundary layer surrounding the sample surfaces, (ii) dissociation of oxygen molecules, (iii) adsorption of oxygen atoms at the surfaces, (iv) ionization, (v) transport through surface layers (space charge effects) and (vi) subsequent bulk diffusion of oxygen vacancies $V_O^{\cdot\cdot}$. This scheme of reactions might be even more detailed, if not intricate [14–17].

The influence of (i) is only observed at higher frequencies and/or for very thin samples when diffusion processes in the gas phase cause a significant delay in the response times. It shall be neglected in the following. The kinetics of the elementary steps (ii)–(v) are not known in detail, therefore they are summarized as one *surface transfer reaction* which takes place previous to *bulk diffusion* (vi). Thus, the oxygen incorporation is virtually reduced to a two-step process. The rate of the slower step determines the kinetics of the overall process and thus the response behavior of the sensor.

Due to charge compensation effects within the anion or cation sublattices, doping influences the kinetic behavior. The materials system $SrTi_{1-x}Fe_xO_3$ in particular shows distinct features suggesting its application as a fast oxygen sensor with response times down to the figure of merit 10 ms when employed in thick film technology [18–22]. For sake of mathematical simplicity however, this paper deals with (nominally) undoped $SrTiO_3$ single crystals as well-defined model system. In reality though, these all show a slight acceptor content due to impurities.

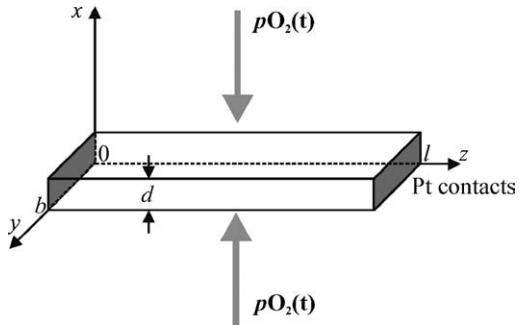

Fig. 1. Geometry of the sample: The two abutting faces of the $SrTiO_3$ single crystal are Pt-contacted, the other four surfaces are exposed to the ambient time-dependent pO_2.

Figure 1 shows the system under consideration. An electrically contacted sample is exposed to a harmonically modulated $pO_2(t)$. In the case of sufficiently small excitation the sensor characteristic can be linearized: By applying only small pressure changes ($pO_2(t) = pO_2^{(0)} + pO_2^{(1)} \sin \omega t$, $pO_2^{(1)} \ll pO_2^{(0)}$), linear system behavior is ensured. Owing to the cubic crystal symmetry, diffusion of $V_O^{\cdot\cdot}$ shall be assumed to take place with the same chemical diffusion coefficient $\tilde{D}_{V_O^{\cdot\cdot}}$ in all directions within the solid.

In the following we shall treat two borderline cases separately: the kinetics of oxygen incorporation being controlled by bulk diffusion or by surface transfer. These can be pictured as "bottleneck" situations in which the reaction rate of one step is far bigger than that of the other.

2.1. Bulk Diffusion Control

The response behavior of the bulk sample, i.e. the kinetics of its conductance change due to a harmonic pO_2 variation, is determined by the bulk diffusion of oxygen vacancies. Oxygen transfer through the boundary surfaces according to Eq. (1) is assumed to occur sufficiently fast. The concentration of oxygen vacancies $[V_O^{\cdot\cdot}]$ can be expressed by Fick's second law:

$$\frac{\partial}{\partial t}\left[V_O^{\cdot\cdot}\right] = \operatorname{div}\left(\tilde{D}_{V_O^{\cdot\cdot}} \operatorname{grad}\left[V_O^{\cdot\cdot}\right]\right) \tag{3}$$

At elevated pO_2, defect chemical considerations taking into account charge compensation effects [23] result in $2[V_O^{\cdot\cdot}] \approx N'_A - p$, N'_A being the (constant)

acceptor and p the hole concentration. The influence, especially at lower temperatures, of trapping effects taking place in Fe-doped $SrTiO_3$ [9, 24, 25] is neglected in this regard. As a result, Eq. (3) can be modified:

$$\frac{\partial p}{\partial t} = \operatorname{div}\left(\tilde{D}_{V_O^{\cdot\cdot}} \operatorname{grad} p\right) \tag{4}$$

Considering samples with lateral dimensions far bigger than their thickness ($b, l \gg d$), a one-dimensional approach is justified:

$$\frac{\partial p}{\partial t} = \tilde{D}_{V_O^{\cdot\cdot}} \frac{\partial^2 p}{\partial x^2} \tag{5}$$

Harmonic pO_2 changes in the gas phase lead to a harmonic modulation of the hole concentration $p(x, t) = p_0 \sin \omega t$ for both major sample surfaces at $x = 0$ and $x = d$. The partial differential Eq. (5) can be reduced to an ordinary one by applying the Laplace transformation:

$$\frac{\mathrm{d}^2 P}{\mathrm{d}x^2} - \frac{s}{\tilde{D}_{V_O^{\cdot\cdot}}} P = 0, \tag{6}$$

$P(x, s)$ being the Laplace transform of $p(x, t)$. Considering the Dirichlet boundary conditions described above for the time domain, Eq. (6) can readily be solved. The resulting $P(x, s)$ must then be integrated over the sample thickness in order to obtain a value for the mean hole concentration in the sample $\overline{P}(s) = {}^1\!/_d \int_0^d P(x, s)\,\mathrm{d}x$ which is directly proportional to the sample conductance (the measurand) or, accordingly, the mean value $\overline{\sigma}(s)$ of the material's electrical conductivity. Since the direction of the field current during conductivity measurements is perpendicular to the diffusion current, the latter is considered not to be affected by the former.

Given $s = i\omega$ (i being the imaginary unit), $\overline{\sigma}$ is a complex function of the angular frequency ω of modulation. The ratio between output and input signals in the frequency domain then defines a complex transfer function or frequency response G:

$$G(i\omega) = \frac{\overline{\sigma}(i\omega)}{P_{O_2}(i\omega)}, \tag{7}$$

$P_{O_2}(i\omega)$ being the frequency transform of the input partial sine pressure signal. Since the system is linear, a harmonic input signal $pO_2(t) \propto \sin \omega t$ will result in a harmonic output $\sigma(t) \propto |G(i\omega)| \cdot \sin(\omega t + \Delta\varphi)$, $|G(i\omega)| = \sqrt{[\mathrm{Re}G(i\omega)]^2 + [\mathrm{Im}G(i\omega)]^2}$ being the amplitude and $\Delta\varphi = \arctan(\mathrm{Im}G(i\omega)/\mathrm{Re}G(i\omega))$ the phase shift of G. For the simple case just considered, $G(i\omega) \propto 1/\sqrt{i\omega d^2/4\tilde{D}_{V_O^{\cdot\cdot}}} \times \tanh \sqrt{i\omega d^2/4\tilde{D}_{V_O^{\cdot\cdot}}}$.

For very thick samples ($d > 0.1 \cdot b$), d being the thickness and b the width (cf. Fig. 1), a correction must be taken into account as the influence of the two remaining sample surfaces exposed to the ambient atmosphere can no longer be neglected. The third dimension of the sample is still considered to be large in comparison with the other two ($l \gg d, b$). A two-dimensional diffusion calculus for this geometry of a rectangular parallelepiped is to be found in the literature [26]. The single solutions for each of the four surfaces penetrated by oxygen are derived under the boundary conditions $P\ (x = 0, 0 < y < b, 0 < z < l) = const.$ (and, accordingly, for the three other surfaces to be considered). These solutions are then superposed to form the overall solution for the transfer function which is given by

$$G(i\omega) = G_0 \sum_{\nu=0}^{\infty} \frac{\tanh\left(\frac{d}{2}\xi\right)}{(2\nu+1)^2 \xi}, \quad \text{with}$$
$$\xi = \sqrt{\frac{(2\nu+1)^2\pi^2}{b^2} + \frac{i\omega}{\tilde{D}_{V_O^{\cdot\cdot}}}}, \tag{8}$$

G_0 being a constant. Only the shape of the transfer function amplitude $|G(i\omega)|$ is of interest. This renders the constant insignificant; for convenience $|G(i\omega)|$ henceforth denotes the normalized amplitude ($|G(0)| \stackrel{!}{=} 1$). As shown in Fig. 2, $|G(i\omega)|$, plotted as a function of the angular frequency of modulation on a

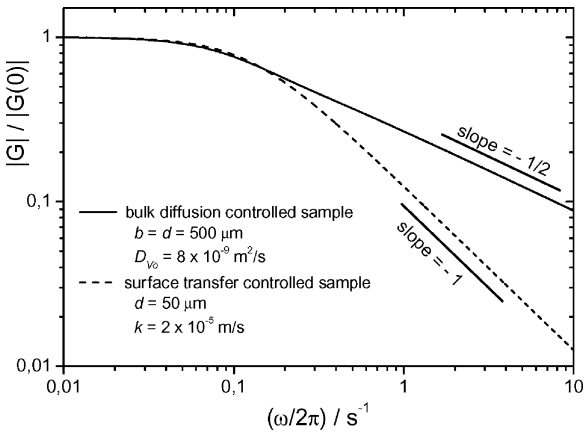

Fig. 2. Amplitude $|G|$ of calculated transfer functions in the case of bulk diffusion controlled (solid curve) and surface reaction controlled kinetics (dashed curve).

double-logarithmic scale (Bode plot), decreases with a slope of $-1/2$ (neglecting dimensions). As remains to be seen, this is the noteworthy result of the calculation. The phase shift shall not be treated any further, as it does not provide any additional information. Besides, it exhibits significant behavior only at higher frequencies, where it is measurable but with difficulty due to the diminishing values of the signals.

2.2. *Surface Transfer Control*

If the oxygen surface transfer reaction (1) is rate-determining for the response behavior of the sample, then a one-dimensional treatment is justified because surface transfer control must occur only for sufficiently thin samples. The basic approach thus consists of solving Fick's second law (5) with suitable boundary conditions again. These arise from the following considerations. Throughout the surface transfer reaction

$$O_2 + 2V_O^{\cdot\cdot} \rightleftharpoons 2O_O^x + 4h^{\cdot} \tag{9}$$

which takes place at $x = 0$ and $x = d$, $[V_O^{\cdot\cdot}]$ and $[O_O^x]$ remain nearly constant [12]. The more O_2 molecules reach the surface, the faster the oxygen incorporation proceeds. Assuming all changes to the system are small, the forward reaction rate r_f of (9) should then, as a first-order approximation, be proportional to the concentration of gas molecules at the surface: $r_f \propto [O_2]|_{x=0,d}$. The backward reaction rate r_b of (9) should accordingly only depend on the hole concentration p at the surface. To simplify matters, this relationship is also linearized by a first-order approach:[1] $r_b \propto p|_{x=0,d}$. A difference between r_f and r_b must result in a diffusion current of oxygen vacancies to or from the surface. Since the latter is coupled with the hole current, these considerations lead to:

$$k_f[O_2]|_{x=0} - k_b p|_{x=0} = -\tilde{D}_{V_O^{\cdot\cdot}} \left.\frac{\partial p}{\partial x}\right|_{x=0} \tag{10}$$

at the sample surface at $x = 0$. Eq. (10) describes a net flux density of particles through the surface in x-direction in a simple linear approach. k_f and k_b are constants of proportionality. They are interrelated through the equilibrium concentrations $[O_2]$ and p when r_f equals r_b [12].

The conditions are the same for the second sample surface at $x = d$. So, for symmetry reasons, a further boundary condition reads:

$$\left.\frac{\partial p}{\partial x}\right|_{x=\frac{d}{2}} = 0 \tag{11}$$

We shall turn to the frequency domain again. Solving Eq. (6) with the boundary conditions given by the frequency transforms of Eqs. (10) and (11), and subsequently integrating over the sample thickness d, leads to a solution for the frequency response which reads:

$$G(i\omega) = G_1 \sinh\left(\frac{d}{2}\Omega\right) \times \left[\Omega \cdot \cosh\left(\frac{d}{2}\Omega\right) + \frac{i\omega}{k} \cdot \sinh\left(\frac{d}{2}\Omega\right)\right]^{-1} \tag{12}$$

with $\Omega = \sqrt{i\omega/\tilde{D}_{V_O^{\cdot\cdot}}}$ and $k := k_b$.[2] G_1 is, as above, a constant without further significance. If surface transfer dominates the kinetic behavior, very fast bulk diffusion can be assumed, corresponding to a diminishing influence of $\tilde{D}_{V_O^{\cdot\cdot}}$ in Eq. (12). The response behavior is that of a first-order low-pass filter with its well-known transfer function depicted in Fig. 2 (dashed curve). In contrast to bulk diffusion controlled kinetics, the amplitude of the response signal, plotted as a function of modulation frequency in a Bode plot, decreases with a slope of –1 (neglecting dimensions).

By means of an analysis of the system's frequency response, it should therefore be possible to clearly distinguish between bulk diffusion or surface transfer reaction as rate-determining processes for real samples. The Bode plot in the former case decreases with a slope of –1/2, in the latter with –1. Furthermore, the cut-off frequency ω_{co}, corresponding to a 3 dB attenuation, is proportional to the reciprocal of the sample's t_{90} time.

3. Experimental

3.1. *Samples*

Single crystal $SrTiO_3$ substrates from CrysTec, Berlin, Germany, and $SrTiO_3$ single crystals from Verneuil-grown boules by Litzenberger, Idar-Oberstein, Germany, both nominally undoped, were used. Conductivity measurements and defect-chemical modelling yielded natural acceptor contents in the order of $N_A \approx 10^{18}$ cm^{-3}. The crystals presented here

were cut to thin slabs with thicknesses of 44 μm, 75 μm (lateral dimensions in the order of 10 mm) as well as a thick sample with a thickness of 5.83 mm and a width of 10.33 mm. The samples were polished with diamond spray, electrically contacted with Pt paste and fired at 1100°C in air for half an hour.

3.2. *Measurement Setup*

A fast kinetic measurement setup first presented and described in [12, 13] was used. pO_2 is periodically changed with an angular frequency ω by varying the total gas pressure $p_{gas}(t)$ instead of the oxygen-gas ratio x_{O_2} so that $pO_2(t) = x_{O_2} \cdot p_{gas}(t)$, $x_{O_2} = 0...100\%$. This is achieved by means of alternatively activated magnetic valves with an angular frequency ω up to 300 s^{-1}. The base line oxygen-gas ratio in the experiments performed was $x_{O_2} = 21\%$. The sample can be heated up to 1000°C. pO_2 is measured by a reference pressure sensor. In order to ensure linear system behavior, the periodic pressure changes were in the order of 1...10% of the mean pressure. Recently, a similar method was employed by Izu et al. [27] for investigating the response behavior of oxygen gas sensors based on cerium oxide thick films.

4. Results and Discussion

For the purpose of an experimental validation of the model presented in this paper, the frequency responses of the samples described in the last section were measured. Figures 3 and 4 show the Bode plots of the frequency responses of two single crystals with different thicknesses (5830 μm and 44 μm, respectively) measured at temperatures in the range from 700...1000°C, in comparison to calculated amplitude values according to (8) and (12), respectively. Due to their conspicuous slopes, the curves can clearly be assigned to the cases of bulk diffusion (thick sample) or surface transfer reaction (thin sample) dominating the kinetics, respectively. The in situ frequency-domain analysis method obviously allows a discrimination between behavior either controlled by bulk diffusion or by surface transfer reaction, in perfect accordance with the model.

Furthermore, it is possible to calculate the chemical diffusion coefficients from the kinetic response data, by varying the parameters $\tilde{D}_{V_O^{\cdot\cdot}}$ and k and fitting calculated

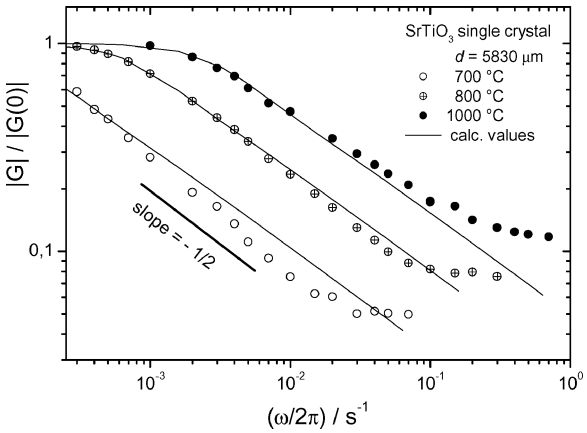

Fig. 3. Amplitude $|G|$ of transfer function calculated from measured frequency response of thick $SrTiO_3$ single crystal ($d = 5830$ μm) as a function of angular frequency ω of modulation at different temperatures. The kinetic behavior of the sample can clearly be identified as bulk diffusion controlled.

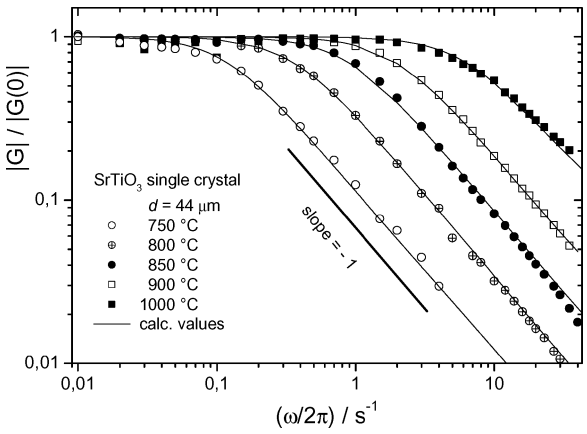

Fig. 4. Amplitude $|G|$ of transfer function calculated from measured frequency response of very thin $SrTiO_3$ single crystal ($d = 44$ μm) as a function of angular frequency ω of modulation at different temperatures. The kinetic behavior of the sample can clearly be identified as surface transfer controlled.

response curves to the measured data. For sufficiently thick samples, there is no influence of k (cf. Eq. (8)), which allows the determination of $\tilde{D}_{V_O^{\cdot\cdot}}$ at different temperatures. Using these values, it is then possible to extract the surface rate constants k from further measurements conducted on very thin crystals. It remains to be stated, however, that only samples with thicknesses in the order of several mm or more are clearly bulk diffusion controlled. The amount of oxygen which can be

incorporated into the sample depends on its volume. With thicknesses decreasing, the surface-to-volume ratio steadily increases. Therefore, the surface reaction is eventually expected to completely control the kinetic behavior [13]. However, this is only the case for very thin samples ($d \approx 50\ \mu$m) in the temperature range under consideration. For thicknesses in between these limits, the influence of both mechanisms can be observed.

Moreover, a distinct temperature dependence is found: At sufficiently high temperatures, surface transfer occurs fast enough, so that the subsequent bulk diffusion becomes rate-determining. At reduced temperatures ($T < 800$°C) however, the surface transfer reaction is slowed down which makes it the rate-determining step. Figure 5 illustrates this behavior for a sample with 75 μm thickness. This temperature dependence must be ascribed to an inhibited surface transfer of oxygen at lower temperatures. The rate of at least one of the elementary transfer reaction steps discussed in Section 2 can be assumed to be considerably decreased, therefore decelerating the overall oxygen incorporation kinetics. Several investigations as to which elementary surface transfer reaction step is responsible for this behavior, as well as the search for surface treatments capable of augmenting the reaction rate of this specific step, are reported in the literature [17].

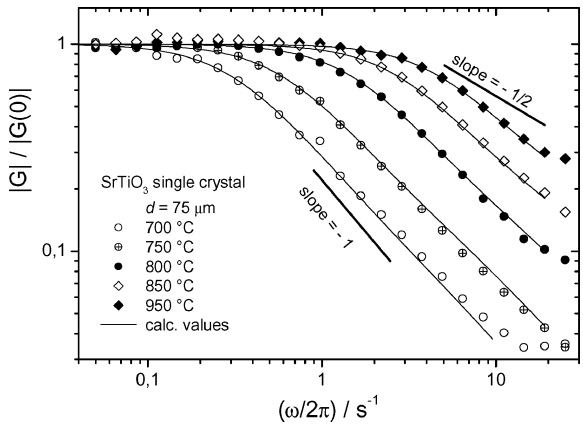

Fig. 5. Amplitude $|G|$ of transfer function calculated from measured frequency response of $SrTiO_3$ single crystal with thickness $d = 75\ \mu$m as a function of angular frequency ω of modulation at different temperatures. A change from basically bulk diffusion controlled kinetics to predominantly surface transfer controlled can be observed with decreasing temperature. Note that the crystals were supplied by different manufacturers which accounts for the higher cut-off frequency (faster response) of this crystal despite its greater thickness compared to the sample in Fig. 4.

5. Conclusions

The frequency-domain analysis, in combination with the in situ kinetic measurement setup described in [12, 13], is not only capable of measuring very short response times, but obviously of providing information on the kinetic behavior the sample shows in response to a pO_2 change, too. This makes it a powerful tool for the investigation of the kinetics of oxygen incorporation into sensor materials.

Notes

1. Applying a mass-action law to Eq. (9) leads to a non-linear dependence: r_b should obviously be proportional to p^4, but due to the assumption of small changes this relationship can be approximated, putting it in formal terms, by expansion into a Taylor series and stopping after the first-order term.
2. Note that k, as defined by Eq. (10), has the dimension of a velocity.

References

1. N.-H. Chan, R.K. Sharma, and D.M. Smyth, *J. Electrochem. Soc.*, **128**, 1762 (1981).
2. U. Balachandran and N.G. Eror, *J. Solid State Chem.*, **39**, 351 (1981).
3. G.M. Choi and H.L. Tuller, *J. Am. Ceram. Soc.*, **71**, 201 (1988).
4. A. Müller and K.H. Härdtl, *Appl. Phys. A*, **49**, 75 (1989).
5. R. Waser, T. Baiatu, and K. H. Härdtl, *J. Am. Ceram. Soc.*, **73**, 1645 (1990).
6. R. Waser, T. Baiatu, and K.H. Härdtl, *J. Am. Ceram. Soc.*, **73**, 1654 (1990).
7. T. Baiatu, R. Waser, and K.H. Härdtl, *J. Am. Ceram. Soc.*, **73**, 1663 (1990).
8. R. Waser, *J. Am. Ceram. Soc.*, **74**, 1934 (1991).
9. T. Bieger, J. Maier, and R. Waser, *Sensors and Actuators B*, **7**, 763 (1992).
10. I. Denk, W. Münch, and J. Maier, *J. Am. Ceram. Soc.*, **78**, 3265 (1995).
11. R. Moos and K.H. Härdtl, *J. Am. Ceram. Soc.*, **80**, 2549 (1997).
12. Ch. Tragut and K.H. Härdtl, *Sensors and Actuators B*, **4**, 425 (1991).
13. C. Tragut, *Sensors and Actuators B*, **7**, 742 (1992).
14. J. Maier, *Solid State Ionics*, **112**, 197 (1998).
15. J. Maier, J. Jamnik, and M. Leonhardt, *Solid State Ionics*, **129**, 25 (2000).
16. J. Maier, *Solid State Ionics*, **135**, 575 (2000).

17. R. Merkle and J. Maier, *Phys. Chem. Chem. Phys.*, **4**, 4140 (2002).
18. J. Gerblinger, K.H. Härdtl, H. Meixner, and R. Aigner, in *Sensors, A Comprehensive Survey*, edited by W. Göpel, J. Hesse, and J.N. Zemel (VCH, Weinheim, 1995), Vol. 8, p. 181.
19. W. Menesklou, H.-J. Schreiner, K.H. Härdtl, and E. Ivers-Tiffée, *Sensors and Actuators B*, **59**, 184 (1999).
20. W. Menesklou, H.-J. Schreiner, R. Moos, K.H. Härdtl, and E. Ivers-Tiffée, in *Materials for Smart Systems III* (*Mat. Res. Soc. Symp. Proc.*), edited by M. Wun-Fogle, K. Uchino, Y. Ito, and R. Gotthardt (Materials Research Society, Warrendale, PA, 2000), Vol. 604, p. 305.
21. E. Ivers-Tiffée, K.H. Härdtl, W. Menesklou, and J. Riegel, *Electrochimica Acta*, **47**, 807 (2001).
22. R. Moos, F. Rettig, A. Hürland, and C. Plog, *Sensors and Actuators B*, **93**, 43 (2003).
23. C. Tragut, *Kinetik schneller Sauerstoffsensoren* (VDI-Verlag, Düsseldorf, 1992).
24. J. Maier, *J. Am. Ceram. Soc.*, **76**, 1223 (1993).
25. R. Waser, T. Bieger, and J. Maier, *Solid State Comm.*, **76**, 1077 (1990).
26. H.S. Carslaw and J.C. Jaeger, *Conduction of Heat in Solids*, 2nd ed. (Clarendon Press, Oxford, 1959), p. 416 ff.
27. N. Izu, W. Shin, and N. Murayama, *Sensors and Actuators B*, **93**, 449 (2003).